Published in final edited form as:
NMR Biomed. 2014 April ; 27(4): 406–416. doi:10.1002/nbm.3075.

On the origins of chemical exchange saturation transfer (CEST) contrast in tumors at 9.4T

Junzhong Xu[a,b,*], **Moritz Zaiss**[c], **Zhongliang Zu**[a,b], **Hua Li**[a,d], **Jingping Xie**[a,b], **Daniel F. Gochberg**[a,b,d], **Peter Bachert**[c], and **John C. Gore**[a,b,d,e,f]

[a]Institute of Imaging Science, Vanderbilt University, Nashville, TN 37232, USA

[b]Department of Radiology and Radiological Sciences, Vanderbilt University, Nashville, TN 37232, USA

[c]Department of Medical Physics in Radiology, Deutsches Krebsforschungszentrum (DKFZ, German Cancer Research Center), Im Neuenheimer Feld 280, D-69120 Heidelberg, Germany

[d]Department of Physics and Astronomy, Vanderbilt University, Nashville, TN 37232, USA

[e]Department of Biomedical Engineering, Vanderbilt University, Nashville, TN 37232, USA

[f]Department of Molecular Physiology and Biophysics, Vanderbilt University, Nashville, TN 37232, USA

Abstract

Chemical exchange saturation transfer (CEST) provides an indirect means to detect exchangeable protons within tissues through their effects on the water signal. Previous studies have suggested that amide proton transfer (APT) imaging, a specific form of CEST, detects endogenous amide protons with a resonance frequency offset 3.5 ppm downfield from water, and thus may be sensitive to variations of mobile proteins/peptides in tumors. However, since CEST measurements are influenced by various confounding effects, such as spillover saturation, magnetization transfer (MT) and MT asymmetry, the mechanism or degree of increased APT signal in tumors are not certain. In addition to APT, nuclear Overhauser enhancement (NOE) effects upfield from water may also provide distinct information about tissue composition. In the current study, APT, NOE and several other magnetic resonance parameters were measured and compared comprehensively in order to elucidate the origins of APT and NOE contrasts in tumors at 9.4T. In addition to conventional CEST methods, a new intrinsic inverse metric was applied to correct for relaxation and other effects. After corrections for spillover, MT and T_1 effects, corrected APT in tumors was found not significantly different from normal tissues, but corrected NOE effects in tumors showed significant decreases compared with normal tissues. Biochemical measurements verified that there is no significant enhancement of protein contents in the tumors studied, consistent with corrected APT measurements and previous literature while qMT data showed decreases in the fractions of immobile macromolecules in tumors. Our results may assist better understanding the contrast depicted by CEST imaging in tumors, and the development of improved APT and NOE measurements for cancer imaging.

Keywords

CEST; APT; NOE; protein concentration; relaxation; exchange; AREX

[*]**Corresponding author**: Vanderbilt University Institute of Imaging Science, 1161 21st Avenue South, AA 1105 MCN, Nashville, TN 37232-2310, USA. Tel.: +1 615 322 8359; Fax: +1 615 322 0734. junzhong.xu@vanderbilt.edu (J. Xu).

Introduction

Chemical exchange saturation transfer (CEST) imaging provides a unique contrast mechanism that reflects the presence of specific chemical groups through indirect measurements of water signal changes due to chemical exchange with saturated solute protons (1–4). Although the concentrations of these small solute pools in biological tissues are usually only in the millimolar range, a large signal enhancement can be achieved through the accumulated effects of the chemical exchange between water and the saturated protons as long as experimental parameters are chosen appropriately. In CEST experiments, spectra are usually acquired with irradiation pulses set over a range of frequency offsets around the water resonance. Normalized by the corresponding unsaturated signal (S_0), a Z-spectrum, (namely, $Z(\Delta\omega) = S(\Delta\omega) / S_0$, where $S(\Delta\omega)$ is the signal measured with saturation at offset $\Delta\omega$) can be obtained in order to identify CEST effects from specific solute pools. For example, amide proton transfer (APT), a specific form of CEST, is believed to reflect the endogenous amide protons with a resonance frequency offset at 3.5 ppm downfield from water, and thus may be sensitive to variations of mobile proteins/peptides (5–8).

APT measurements, like all CEST data, depend in practice on multiple other effects, including magnetization transfer (MT) with broad macromolecular resonances, asymmetry in the MT lineshapes, and water longitudinal relaxation (9). To quantify the APT effect, an asymmetric analysis is often performed by subtracting the signals acquired with saturation on the solute (the label scan) from that on the other side of water (the reference scan) (3). However, this method is sensitive to B_0 inhomogeneities and may also be affected by various other confounding parameters. To avoid these effects, several alternative methods have been proposed. The three-offset method (APT*) subtracts the label scan signal and the average of two nearby acquisitions (10). Chemical exchange rotation transfer (CERT) subtracts two pulsed-CEST signals at two different irradiation flip angles, but with the same average power and frequency offset (11). The saturation with frequency alternating RF irradiation (SAFARI) method has also been proposed to remove the MT effect and MT asymmetry (12). However, none of these methods correct the effect of water relaxation, which can have a major influence on the magnitudes of CEST signals. Recently, Zaiss et al. have proposed an intrinsic inverse metric for Z-spectrum evaluation to correct for spillover and MT dilution of CEST effects, and a further correction can remove the influence of water longitudinal relaxation (13).

Proteins and peptides play important roles in cellular activities, so APT imaging can potentially provide a non-invasive means to characterize abnormal tissues such as tumors without exogenous probes and radiation. For example, APT has been found to be a promising imaging indicator for detecting brain tumors, grading of gliomas, and differentiation of radiation necrosis from active/recurrent tumors (6–8). In brain tumors, the observed APT signals are usually found increased compared to normal tissues, which has been explained as a possible over-expression of proteins/peptides in malignant tissues. However, CEST measurements may be influenced by many confounding effects, the mechanism of increased APT signal in tumors is not clear. To complicate matters, a recent study indicated that APT contrast assessed using a conventional asymmetric analysis is actually a mixture of APT and nuclear Overhauser enhancement (NOE) effects (14). Moreover, it has been long well-known that the water content is usually higher in tumors (15), and the macromolecular content is more dilute in rapidly growing tissues like tumors (16–18), and these characteristics have been invoked in the past to explain the well-established finding that T_1 is usually significantly enhanced in tumors (19,20). It is therefore questionable how well APT reflects the concentration of proteins/peptides in tissues. However, potentially the origins of APT contrast in tumors may be elucidated using multiple MR parameters and protein measurements.

In addition to chemical exchange with downfield protons, nuclear Overhauser enhancement (NOE) effects in the upfield NMR spectral range of aliphatic and olefinic protons, ranging from −5 to 0 ppm relative to water in the Z-spectrum, may also affect water signals. It has been shown that NOE-based signals measured in this spectral range can arise from mobile macromolecular components such as mobile proteins and lipids (21–24). Via direct through-space dipolar coupling (10,25) or mediated by other exchangeable protons (4), NOE signals originating from the non-exchangeable protons in such mobile macromolecular components may provide distinct information on molecular composition. Recently, Liu et al. used a four-pool model to quantify NOE effects in human brain at 7T and found white matter shows much stronger NOE couplings compared with gray matter (26). Mougin et al. also found NOE signals are more sensitive to myelination than the MT signal (27). In addition, a recent study suggests protein unfolding can lead to NOE signal drop (28). However, like APT, NOE measurements are also sensitive to similar confounding influences, such as relaxation, MT effects and asymmetry, and overlapping lipid resonances from subcutaneous adipose tissue, which make quantification difficult. Jin et al. developed a three-offset method (NOE*) which subtracts the measured NOE signal and the average of two nearby measured signals to avoid the MT asymmetry effect (10). However, this method is still influenced by T_1, T_2 and conventional MT effects. Jones et al. found a slight decrease in the NOE effect in human brain tumors by using a fitting method at very low irradiation powers (21). This method is less influenced by conventional MT and MT asymmetry. However, as very low power was used, the contrast between tumor and normal tissue is also low. Overall, a more reliable method to quantify NOE effects is needed.

In the current study, we measured APT, NOE and several other MR parameters in order to elucidate the origins of APT and NOE contrasts in tumors at 9.4T comprehensively. In addition to the conventional CEST quantification methods, i.e. asymmetric analysis for APT (5) and three-offset method for APT and NOE (10), we also implemented a new intrinsic inverse metric 1/Z of the Z-spectrum to quantify the contrast of the NOE effect in tumors. This method is based on the equivalence of spin-lock and CEST experiments, and with correction of spin-lattice relaxation rate R_1, it has been shown to provide a more direct exchange-weighted contrast with much reduced influence from other confounding effects (13). The APT and NOE values from these different methods were correlated to multiple conventional MR parameters (R_1, R_2, PSR (pool size ratio of macromolecular pool obtained in quantitative magnetization transfer (qMT) measurements), k_{mf} (MT exchange rate from macromolecular pool to free water pool obtained in qMT), and ADC (apparent diffusion coefficient)). Finally, the protein concentrations in tumors and contralateral normal brain tissues were quantified using two biochemical methods (Bradford (29) and BCA (30) methods), and compared with APT values. Our results may assist better understanding the contrast depicted by CEST imaging in tumors, and assist the development of improved APT and NOE measurements in cancer imaging.

Materials and methods

Conventional quantification of APT and NOE

APT contrast is usually characterized by measuring CEST asymmetry, which subtracts the signals acquired with saturation at the amide frequency offset 3.5 ppm from that on the other side of water −3.5 ppm (reference scan) (5), namely

$$MTR_{asym}(3.5ppm)=Z(-3.5ppm)-Z(3.5ppm) \quad [1]$$

Note that all frequency offsets are relative to the water resonance. Hence, since water and the MT macromolecules have different resonant frequencies, this metric also incorporates

any asymmetry of MT. To reduce this effect, a three-offset method (10) was proposed recently,

$$APT*=Z_{ref}(3.5ppm)-Z(3.5ppm), \quad [2]$$

where Z_{ref} (3.5*ppm*) = [*Z*(4.0 *ppm*) + *Z*(3.0 *ppm*)] / 2. Note that APT* avoids the influence of any NOE effect at −3.5 ppm, and may also reduce the dependence on MT asymmetry.

To quantify the NOE effect, Jin et al. proposed a similar three-offset method (10), namely,

$$NOE*=Z_{ref}(-3.5ppm)-Z(-3.5ppm), \quad [3]$$

where Z_{ref} (− 3.5*ppm*) = [*Z*(− 2.0 *ppm*) + *Z*(− 5.0 *ppm*)] / 2. Figure 1 illustrates an example of how APT* and NOE* are obtained based on a representative Z-spectrum of a rat 9L glioma tumor.

1/Z method

A different approach was recently proposed by Zaiss and Bachert based on the equivalence of spinlock (SL) and CEST experiments (13). Consider two exchanging pools *a* (water) and *b* (amide or other exchanging species with a chemical shift $\Delta\omega_{lab}$ relative to water) that have longitudinal relaxation rates R_{1a} and R_{1b}, transvers relaxation rates R_{2a} and R_{2b}, chemical exchange rates k_a (from *a* to *b*) and k_b (from *b* to *a*), and proton fractions relative to water pool, i.e. f_a =1 and $f_b = k_a / k_b$. If the magnetization reaches steady-state after saturation, the Z-spectrum is given by (13)

$$Z(\Delta\omega)=\frac{S(\Delta\omega)}{S_0}=\cos^2\theta\cdot\frac{R_{1a}}{R_{eff}(\Delta\omega)+R_{ex}(\Delta\omega)}, \quad [4]$$

where θ is the angle between the effective field $\vec{\omega_{eff}}$ = (ω_1, 0,Δω) and z-axis, i.e. θ = $\tan^{-1}(\gamma B_1/\Delta\omega)$, R_{eff}(Δω) corresponds to the relaxation rate of the water pool in the rotating frame,

$$R_{eff}(\Delta\omega)=R_{1a}\cos^2\theta+R_{2a}\sin^2\theta, \quad [5]$$

and R_{ex}(Δω) is the exchange-dependent relaxation rate which is approximately described by a Lorentzian function with the peak at the CEST pool resonance $\Delta\omega_{lab}$, namely

$$R_{ex}(\Delta\omega)=\frac{R_{ex}^{lab}\Gamma^2/4}{\Gamma^2/4+(\Delta\omega-\Delta\omega_{lab})^2}, \quad [6]$$

where Γ is the full width at half maximum which can be expressed as

$$\Gamma=2\sqrt{\frac{k_b+R_{2b}}{k_b}\omega_1{}^2+(k_b+R_{2b})^2}, \quad [7]$$

and R_{ex}^{lab} is the amplitude of the Lorentzian function

$$R_{ex}^{lab}=f_b k_b\frac{\omega_1^2}{\omega_1^2+k_b(k_b+R_{2b})}. \quad [8]$$

Note that in the full-saturation limit, i.e. $\omega_1^2 \gg k_b(k_b + R_{2b})$, Eq.[8] can be simplified as

$$R_{ex}^{lab} \approx f_b k_b = k_a. \quad [9]$$

Therefore, $R_{ex}(\Delta\omega_{lab}) = R_{ex}^{lab} \approx f_b k_b$ is an intrinsic parameter which forms the origin of the CEST effect. Note that R_{ex}^{lab} depends on the chemical exchange rate without significant influence from other confounding effects.

In order to obtain R_{ex} ($\Delta\omega_{lab}$ (to isolate the CEST effect), a reference Z-spectrum should be obtained. The most common reference value is the Z-value at the opposite frequency $\Delta\omega_{ref} = -\Delta\omega_{lab}$. The corresponding water contribution is the same, i.e. R_{eff} ($\Delta\omega_{ref}$) = $R_{1a} \cos^2\theta + R_{2a} \sin^2\theta = R_{eff}$ ($\Delta\omega_{lab}$), but R_{ex} ($\Delta\omega_{ref}$) decreases significantly as

$$R_{ex}^{ref} = R_{ex}(-\Delta\omega_{lab}) = \frac{R_{ex}^{lab}\Gamma^2/4}{\Gamma^2/4 + (2\Delta\omega_{lab})^2} \quad [10]$$

For B_1 = 1 μT, B_0 = 9.4T, $\Delta\omega_{lab}$ = 3.5 ppm and R_{2b}, k < 100 Hz, $R_{ex}^{ref} < 0.001 \cdot R_{ex}^{lab}$ and can be neglected. Thus, at the reference frequency

$$Z_{ref}(\Delta\omega_{ref}) = \cos^2\theta \cdot \frac{R_{1a}}{R_{eff}(\Delta\omega_{lab})}, \quad [11]$$

A magnetization transfer rate (MTR) can be defined using both $Z(\Delta\omega_{lab}$ and Z_{ref} ($\Delta\omega_{ref}$). The most common MTR is the above mentioned MTR_{asym}, namely

$$MTR_{asym}(\Delta\omega_{lab}) = Z_{ref}(-\Delta\omega_{lab}) - Z(\Delta\omega_{lab}) = \cos^2\theta \cdot \frac{R_{ex}(\Delta\omega_{lab})R_{1a}}{R_{eff}(\Delta\omega_{lab}) \cdot [R_{eff}(\Delta\omega_{lab}) + R_{ex}(\Delta\omega_{lab})]} \quad [12]$$

$\Delta\omega_{lab}$ = 3.5 ppm in the MT asymmetry analysis of conventional APT contrast. Apparently, a more beneficial way to analyze is to use the subtraction of the inverse Z-values, i.e.

$$MTR_{Rex}(\Delta\omega_{lab}) = \frac{1}{Z(\Delta\omega_{lab})} - \frac{1}{Z_{ref}(\Delta\omega_{ref})} = \frac{R_{ex}(\Delta\omega_{lab})}{\cos^2\theta \cdot R_{1a}} \quad [13]$$

By multiplication by R_{1a}, a new metric which we term apparent exchange-dependent relaxation (AREX) can be achieved without the influence the longitudinal relaxation of water pool, namely

$$AREX(\Delta\omega_{lab}) = MTR_{Rex}(\Delta\omega_{lab}) \cdot R_{1a} = R_{ex}(\Delta\omega_{lab})/\cos^2\theta \quad [14]$$

Revised 1/Z method

The original 1/Z method mentioned above proposes to use the reference value at the opposite frequency for APT quantification analogous to asymmetry analysis (13). In order to further reduce MT asymmetric effect *in vivo*, we propose a revised 1/Z method which combines the original 1/Z method and the three-offset method in the current study. For the APT quantification, instead of taking the reference value at the opposite frequency, we estimate the reference value at 3.5 ppm by the average of two values shifted by δω left and right from the CEST peak at $\Delta\omega_{lab}$, respectively,

$$Z_{ref}(\Delta\omega_{lab})=\frac{Z(\Delta\omega_{lab}+\delta\omega)+Z(\Delta\omega_{lab}-\delta\omega)}{2} \quad [15]$$

At these frequencies,

$$R_{ex}^{ref}=R_{ex}(\Delta\omega_{lab}\pm\delta\omega)=\frac{R_{ex}^{lab}\Gamma^2/4}{\Gamma^2/4+\delta\omega^2} \quad [16]$$

For B_1 = 1 μT, B_0 = 9.4T, δω = 0.5 ppm, and R_{2b}, k < 100 Hz, $R_{ex}^{ref}<0.025\cdot R_{ex}^{lab}$ and can still be neglected. Importantly, this new reference value R_{ex}^{ref} has no contribution from concomitant effects at the opposite frequency that may exist in the original 1/Z method mentioned above. Specifically,

$$\frac{Z(4.0ppm)+Z(3.0ppm)}{2}=Z_{ref}(3.5ppm)=\frac{R_{1a}}{R_{eff}(3.5ppm)}\cdot\cos^2\theta, \quad [17]$$

$$MTR_{Rex}(APT)=\frac{1}{Z(3.5ppm)}-\frac{2}{Z(4.0ppm)+Z(3.0ppm)}=\frac{R_{ex}(APT)}{\cos^2\theta\cdot R_{1a}}, \quad [18]$$

and

$$AREX(APT)=MTR_{Rex}(APT)\cdot R_{1a}=R_{ex}(APT)/\cos^2\theta\approx R_{ex}(APT)=k_a(APT) \quad [19]$$

where k_a^{APT} represents the exchange rate from water to the amide proton pool. Likewise, we define

$$MTR_{Rex}(NOE)=\frac{1}{Z(-3.5ppm)}-\frac{2}{Z(-2.0ppm)+Z(-5.0ppm)}=\frac{R_{ex}(NOE)}{\cos^2\theta\cdot R_{1a}}, \quad [20]$$

and

$$AREX(NOE)=MTR_{Rex}(NOE)\cdot R_{1a}=R_{ex}(NOE)/\cos^2\theta\approx R_{ex}(NOE)=k_a(NOE) \quad [21]$$

where k_a^{NOE} represents the exchange rate from water to the NOE pool. Note that for offsets larger than 2 ppm at field strength 9.4T and B_1 < 2 μT, the term $\cos^2\theta$ is approximately 1 (> 0.99). Therefore, with the parameters used in the current work, AREX is approximately an intrinsic metric that is dependent on the chemical exchange rate with minimized influence from other confounding effects. Figure 1 illustrates how these APT and NOE quantification methods were used with a representative Z-spectrum of a rat 9L glioma tumor.

Animal and cancer model

All animal related procedures were approved by the Institutional Animal Care and Use Committee at Vanderbilt University. 9L glioblastoma cells were obtained from American Type Culture Collection (ATCC 9L/lacZ, CRL-2200) and grown in Dulbecco's modified Eagle's medium (DMEM; Gibco, Gaithersburg, MD) with 10% fetal calf serum and 50 units/ml penicillin and 50 μg/ml streptomycin maintained in a humidified incubator at 37 °C with 5% CO_2. Eight male Fischer 344 rats (250 – 300 grams) were immobilized and anesthetized with a 2%/98% isoflurane/oxygen mixture. Each rat was injected with 1×10^5 9L glioblastoma cells in their right brain hemispheres to allow tumors to grow to 30–40

mm3 after 14 – 18 days. Details of the surgical procedures have been reported previously (18,31).

Animals were anesthetized with 3% isoflurane for induction and 2% thereafter during imaging. The position of each rat head was secured using an MRI compatible cradle with bite and head bars. A warm-air feedback system was used to ensure rat rectal temperature was maintained at ~ 37 °C throughout experiments.

In vivo MR imaging

MR images were acquired on a 9.4T Varian 21-cm-bore horizontal MRI scanner. An RF Litzcage Coil (Doty Scientific Inc., Columbia, SC) with 38 mm internal diameter was used for both transmission and receiving. All of the multiple parametric images including CEST were acquired using the following parameters: a 2-shot spin-echo echo-planar imaging (EPI) sequence with a triple reference imaging method was used to reduce EPI ghost artifacts (32). The number of excitations was 2. A single axial slice crossing the center of the tumor was acquired with a slice thickness of 2 mm. The field-of-view was 32 × 32 mm, and the matrix size was 96 × 96, which yields an isotropic in-plane resolution of 333 μm.

CEST images were acquired with continuous wave saturation pulses (1μT for 5 seconds) with 81 frequency offsets evenly distributed from −5 ppm to 5 ppm relative to water resonance, yielding a high spectral resolution (0.125 ppm). All Z-spectra were obtained with normalization of corresponding unsaturated signals ($\Delta\omega$ = 300 ppm) and corrected for B_0 inhomogeneities using the WASSR method (33). Longitudinal relaxation rate R_1 (= $1/T_1$) was mapped using an inversion recovery and spin-echo EPI sequence with an Adiabatic inversion pulse to reduce the B_1 inhomogeneity effect. Eight inversion times were used (50 ms, 100 ms, 250 ms, 500 ms, 1sec, 1.5 sec, 2 sec and 4 sec). The transverse relaxation rate R_2 (= $1/T_2$) was obtained using a spin-echo EPI sequence with five echo times (30, 40, 60, 80 and 100 ms). Quantitative magnetization transfer (qMT) using a selective inversion recovery (SIR) method (34,35) was used to map the pool size ratio (PSR) and the MT exchange rate from macromolecular pool to free water pool (k_{mf}) assuming the conventional two-pool model of tissue protons. Specifically, a 1-ms 180° hard pulse was used to invert water pool spins prior to the spin-echo EPI readout. A bi-exponential recovery curve was acquired with 16 inversion times logarithmically distributed from 3 ms to 10 sec. The experiments were performed using a recently developed SIR-EPI sequence, which contains a saturation pulse train to significantly accelerate the acquisition but preserves the feature of fitting qMT parameters without bias. Details of this sequence have been reported elsewhere (18). Apparent diffusion coefficients (ADC) were estimated using the conventional pulsed gradient spin echo (PGSE) diffusion sequence with a diffusion gradient duration (δ) of 5 ms and a separation (Δ) of 12 ms, in which a mono-exponential fitting was performed with four b values (400, 600, 800, and 1000 s/mm^2).

Biochemical determination of protein concentration

Immediately after MR imaging, rats were perfused with sterile saline before sacrifice. Rats were decollated with a guillotine and, after removal of skin, whole rat heads were rapidly frozen by immersion in a mixture of hexane and dry ice in order to prevent protein degradation. Frozen rat brains were then dissected at −20 °C into 2 mm thin sections with the aid of a rat brain slicer (Zivic Instruments, Pittsburgh, PA), and 3 pieces of tissues (~ 20 mg weight for each) from the tumors and from the contralateral normal brain were cut out. Total proteins were then extracted with 25× (w/v) of 2% of SDS by homogenization with a 25G needle/syringe and then incubated in 70 °C for 30 minutes (36). Insoluble debris was removed using a microcentrifuge (Biorad, maximum speed for 10 minutes). The total protein extract was then diluted 10 times to reduce SDS concentration for quantification.

Protein concentrations were determined by both Bradford (29) (Bio-rad) and Bicinchoninic acid assay (BCA) (30) methods by following manufacture recommended procedures. To confirm the dissected cancerous tissues originated from the xenografted 9L tumors, tumor and normal cell lysate were separated along with lysate extracted from cultured 9L cells by SDS-PAGE, and then stained with Coomassie brilliant blue. The pattern of protein bands confirmed the accuracy of the dissection of the cancerous and normal tissues.

Data analysis

All data analyses were performed using programs written in Matlab (Mathworks, Natick, MA) except the image registration which was written in C. Our experimental settings constrained any movements along z (slice selective) direction but there might be some small movements in the x–y plane due to respiration. Therefore, all images were coregistered to a corresponding 2-shot spin-echo EPI image with echo time 18 ms using a rigid body registration algorithm by maximizing the normalized mutual information (37). Following co-registration, the brain region was manually selected for further parametric fitting. All MR parameters, including T_1, T_2, PSR, k_{mf}, ADC and all CEST parameters were fitted on a pixel-wise basis without data smoothing. The region-of-interest (ROI) of the tumor of each rat was manually selected on the corresponding T_1 map, which shows a very clear contrast between glioma tumor and normal tissue (see Figure 3). The ROI of the contralateral normal tissue was chosen as the mirrored tumor ROI in the left hemisphere after a slight shifting adjustment to avoid CSF.

Results

Sample CEST spectra

Figure 2 shows representative Z-spectra of a 9L glioma tumor and corresponding contralateral normal tissue. There is a clear APT effect at 3.5 ppm which appears to be larger in the tumor. MTR_{asym} using conventional asymmetry analysis is also shown (solid lines in Figure 2). MTR_{asym} is negative at most frequency offsets except 0 – 1.0 ppm for both tumor and normal tissues, indicating that MTR_{asym} is significantly affected by the MT asymmetry and NOE effects. Interestingly, a distinct NOE peak was also found at −1.6 ppm in contralateral normal tissues only, which vanished in the tumor. The origins of this NOE peak are not clear and are still under investigation.

Multi-parametric maps and correlations

Figure 3 shows multiple MR parametric maps of a representative rat. R_1 shows excellent contrast for distinguishing the tumor from normal brain tissue, and hence all ROIs were manually selected from R_1 maps in the current study. R_2, ADC and PSR also show clear contrasts for detecting tumor. Despite being more sensitive to noise, k_{mf} also shows a clear differentiation of tumor from normal tissue and is higher in the tumor. The different patterns within the tumor reflect the heterogeneous nature of the 9L glioma. MTR_{asym} shows high contrast between tumor and normal tissue, and white matter (corpus callosum) can be clearly distinguished from cortical gray matter, which is consistent with previous findings that the MTR_{asym} contrast between gray matter and white matter is enhanced at higher field (38). APT* obtained using the three-offset method, as well as the MTR_{Rex} obtained using the 1/Z method, also show pronounced contrast between normal brain and tumor, although the imaging contrast between gray matter and white matter decreases. Interestingly, AREX(APT), which is believed to be more specific for detecting variations in composition and exchange rates of mobile proteins and peptides, shows almost no imaging contrast between tumor and normal tissue. NOE* obtained using the three-offset method is slightly enhanced in white matter, but the overall imaging contrast is very small, which is similar to previously reported results (10). Interestingly, though there is no significant contrast of

NOE* to distinguish tumor and normal tissue, the image contrast becomes more clear in the MTR_{Rex}(NOE) map obtained using the revised 1/Z method. After correction for R_1 relaxation, the imaging contrast is more pronounced for detecting tumor.

Fig. 4 shows correlations among the five conventional MRI parameters (R_1, R_2, PSR, k_{mf} and ADC), respectively, of all eight rats. For the correlation of each pair of parameters in each sub-figure, the Spearman's r and p-value are provided. In addition, the corresponding linear regression (solid line) is provided to indicate how these MR parameters are correlated in a linear manner. Tumors show a significant decrease in both R_1 and PSR, showing that tumors have lower levels of macromolecules promoting longitudinal relaxation, consistent with extensive earlier literature and conventional explanations of lower relaxation rates in malignant and other rapidly growing tissues (19). The MT exchange rate, k_{mf}, is significantly higher in tumors, consistent with previous reports (16–18). There is also a small increase in ADC, suggesting a lower cellularity in tumors. By contrast, R_2 was higher in tumors, which differs from results obtained at lower field strengths (20,39), where tumors usually show both decreased longitudinal and transverse relaxation rates. However, this increase is consistent with a model in which dipolar effects between macromolecules and water, which dominate relaxation at lower fields, and which decrease with field strength, become less important compared to chemical exchange contributions to transverse relaxation, which increase with field strength, as demonstrated in diamagnetic protein solutions by Zhong et al. (40). As such, R_2 is expected to increase less strongly with PSR but more strongly with CEST effects. Indeed, in this model R_2 was found to correlate inversely with PSR in the current study ($p = 0.008$), suggesting strongly that R_2 (and by inference CEST effects) no longer reflects gross macromolecular composition but rather other changes in the tumor milieu that promote exchange. This is also consistent with the behavior of k_{mf}, which correlates strongly with R_2. ADC is not correlated with any other conventional MR parameters (the last row in Figure 4), suggesting that relaxation properties are somewhat independent of cell density.

APT

Figure 5 summarizes the correlations between four CEST parameters (MTR_{asym}, APT*, MTR_{Rex}(APT) and AREX(APT)) and five conventional MRI parameters (R_1, R_2, PSR, k_{mf} and ADC), for all eight rats. MTR_{asym}, APT* and MTR_{Rex}(APT) were all higher in tumors, while AREX(APT) was similar in the tumor and contralateral normal tissue, resulting in negligible imaging contrast for detecting the tumor (see Figure 3). MTR_{asym}, APT* and MTR_{Rex}(APT) appear to be significantly inversely correlated with PSR (the Spearman's correlation gives $p = 0.001$, 0.017 and 0.017 respectively), but, after the correction for R_1 relaxation, AREX(APT) has no significant correlation with PSR ($p = 0.617$). Thus CEST metrics corrected for relaxation effects show little connection with direct measures of total macromolecular content, but may appear to correlate when there are corresponding variations in R_1. This is consistent with the left column of Figure 5 in which MTR_{asym}, APT* and MTR_{Rex}(APT) measurements are all significantly correlated with R_1 (p values 0.012, 0.001 and 0.009 respectively) but not with AREX ($p = 0.856$). None of the four APT parameters are strongly correlated with R_2. This is perhaps because APT detects relatively slow chemical exchange from amide protons, whereas R_2 may be affected more by faster chemical exchange from other metabolites such as amine or hydroxyl protons at high field. Hence, APT parameters and R_2 vary independently even though R_2 contains a strong contribution from chemical exchange at this field strength. The fact that there is no different correlation of spillover corrected methods and uncorrected methods may be due to negligible influence of spillover dilution - which increases with R_{2a} - at 9.4T due to the large frequency difference to water. The CEST metrics showed only weak correlations with ADC, except MTR_{asym}.

Figure 6 summarizes the behaviors of all four APT parameters (MTR_{asym}, APT*, MTR_{Rex}(APT) and AREX(APT)) for all eight rats, comparing tumors to normal tissues. Only the conventional MTR_{asym}(APT) show negative values in both tumor and contralateral normal tissue, indicating that there is a significant influence of the MT asymmetric effect in MTR_{asym}(APT). Both APT* and MTR_{Rex}(APT) show significantly higher values in the tumor ($p<0.01$ given by the Wilcoxon rank-sum test). However, AREX(APT), with the correction for R_1 relaxation, shows no significant difference between tumor and normal tissue ($p=0.28$ by the Wilcoxon rank-sum test).

The results of biochemical protein determinations (both Bradford and BCA methods) are provided in Table 1. Using these assays, it was found that tumors had only slightly but not significantly ($p=0.093$ and 0.394 given by Wilcoxon rank-sum test for Bradford and BCA methods, respectively) higher total protein contents compared to contralateral normal brain tissue. The results of APT measurements are also shown in Table 1. It is clear that the small but insignificant variations of protein content between tissues is insufficient to explain the much larger differences in the three APT parameters, MTR_{asym}, APT* and MTR_{Rex}(APT). In contrast, the total protein measurements were consistent with the AREX(APT) measurements, which also show a small but insignificant increase in tumors. This is consistent with the proposition that AREX(APT) is less sensitive to other confounding effects and may be a more robust indicator of protein contents in biological tissues.

NOE

Figure 7 summarizes the correlation of the three NOE parameters (NOE*, MTR_{Rex}(NOE) and AREX(NOE)) with five conventional MRI parameters (R_1, R_2, PSR, k_{mf} and ADC), respectively, for all eight rats. Both MTR_{Rex}(NOE) and AREX(NOE) correlate strongly with PSR ($p = 0.001$) and k_{mf} ($p = 0.001$), indicating these two parameters are directly related to the macromolecular content and magnetization transfer between water and the broad background proton pool. MTR_{Rex}(NOE) and AREX(NOE) are also strongly correlated with R_1 (both $p < 0.001$ by the Spearman's correlation) and inversely with R_2 ($p = 0.035$ and 0.016 respectively). NOE* correlates significantly only with R_1 ($p = 0.042$ by the Spearman's correlation), and no metric is correlated strongly with ADC.

Figure 8 summarizes the behaviors of three NOE parameters from all eight rats, comparing tumors and normal tissue. NOE* obtained using the 3-offset method does not distinguish tumors from contralateral normal tissues ($p = 0.33$ given by the Wilcoxon rank-sum test), whereas both MTR_{Rex}(NOE) and AREX(NOE) show significantly lower values in the tumor compared to normal brain ($p < 0.01$).

Discussion

The measurements of multiple MR parameters and biochemical protein assays presented above were performed in order to better understand the origins of CEST contrast in tumors. The results show that, at least for the tumor type and field strength used in the current study, tumors have lower R_1 and PSR, higher R_2 and k_{mf}, and higher ADC than in contralateral normal tissue. The higher R_2 in tumors is contradictory to the results of the same tumor type reported at lower field strength at 4.7 T (5), but this may be due to the increased contribution of exchange processes, that are more pronounced in tumors, to R_2 at higher field strengths (40). All other results are consistent with previous results at lower field strength and are consistent with a model of tissue water in which R_1 reflects the influence via dipole-dipole couplings of macromolecules in solution on water molecules within hydration layers or otherwise associated with proteins that then undergo rapid exchange with the bulk aqueous phase. Relaxation rates then increase in more concentrated solutions as percentage of water by volume decreases. The differences in R_1 and PSR between tumors and normal brain

confirm that the total macromolecular content relevant for affecting water relaxation is generally lower in tumors than in normal tissue. The observed variations in R_2 at 9.4T suggest there is an increased contribution to transverse relaxation from exchanging protons that more than compensates for the variation of the total protein concentration, either because of a change in the nature of the macromolecules (e.g. decomposition into smaller fragments) or in the exchange rate (which may be affected by pH and molecular conformation). The observed higher values for k_{mf} also indicate the average rate of transfer of magnetization between water and macromolecules increases in these tumors. Higher ADCs in 9L tumors suggest that the cellularity is lower in tumors compared with normal tissue. Our biochemical measurements confirm that the total protein content in 9L glioma tumor is not significantly different from normal brain tissue.

There arises a potential confound in these data in that the PSR derived from qMT shows clear decreases in tumors, whereas total protein measured biochemically is not significantly changed. This discrepancy could reflect differences in the experimental sampling of the tissues, but more likely reflects the fact that not all protein extracted biochemically contributes equally to relaxation, whereas the PSR is an indirect measure of only those immobile components that are available for magnetization transfer.

The intrinsic asymmetry of the Z-spectra associated with semi-solid macromolecules in biological tissues can confound conventional asymmetry analysis and the quantification of APT effects (41). In the current study MTR_{asym} obtained using such an asymmetry analysis produces negative APT contrasts in both tumors and normal tissues. Values of APT* obtained using the three-offset method, and MTR_{Rex}(APT) obtained using the revised 1/Z method, avoid the conventional asymmetry analysis, and produce positive imaging contrasts. In addition, these two parameters show significantly higher values in tumors, but after correction for R_1 relaxation, AREX(APT) shows no significant contrast between tumors and contralateral normal tissues. This suggests that conventional measurements of APT, including MTR_{asym} and APT*, may be significantly "contaminated" by MT asymmetry and/or R_1 effects. MTR_{Rex} corrects for MT effects, but still have a difference between tumors and normal tissues. However, after correcting for such effects, the contrast AREX(APT), between tumor and normal brain tissue disappears, which is consistent with the insignificant difference of the total protein concentration obtained from biochemical measurements. Based on the theory proposed by Zaiss et al. (13), AREX(APT) yields a clean CEST evaluation which is more sensitive to contents and the exchange rate of the APT pool without confounding effects like spillover, MT and R_1 relaxation. At least for the tumor type (9L) and the CEST measurements performed in the current work, the imaging contrast obtained using conventional APT methods, including MTR_{asym} and APT*, may be dominated by effects of R_1.

The NOEs may depend on the applied RF powers. For example, it has been reported that the NOE signal at 4.7T is more pronounced at lower saturation powers and is lower in tumor than in contralateral normal tissue (41). While the NOE effects were reported to peak at a B_1 of ~ 1 – 1.4 μT at 7T (26). In the current study, a relatively large saturation power (1 μT) was used and no significant difference was found between the NOE effects in tumors and those in the contralateral normal tissues. On the other hand, MTR_{Rex}(NOE) obtained using the revised 1/Z method shows significant differences between tumors and normal tissues, and these differences increase for AREX(NOE) if corrections for R_1 relaxation are performed. Moreover, variations in AREX(NOE) between animals correlate strongly with PSR.

Intrinsically, NOEs depend on the average cross-relaxation rate, which is a function of interaction distances and correlation times (42). These parameters are directly related to the

structure and mobility of the observed spins (43). Neglecting the exchange-relayed mechanisms (21), and if we assume the protein concentration to be constant, decreased NOEs indicate either less external or internal motional restrictions. For example, partially unfolded proteins may tumble more freely, mitigating dipole-dipole interactions. A recent study of Zaiss et al. (28) showed that unfolding of proteins lead to decreased NOE signals in the Z-spectrum and might therefore be a possible explanation for the observed NOE drop in tumors and necrosis. However, there is no clear evidence in our data that the principle mechanism is protein unfolding, as its influence on APT and other MR parameters is not yet understood, and the lowered NOE (combined with longer T_1 and lower PSR) is also consistent with diminished external structure allowing the whole protein to tumble more freely, i.e. a more liquid environment.

The remarkable influence of R_1 relaxation on both APT and NOE measurements indicates the need for mapping and correcting for variations in relaxation rates to obtain reliable CEST measurements, as shown in this paper and other studies (44,45). By contrast, AREX is an exchange-rate dependent parameter which is insensitive to spillover, MT and R_1 relaxation and hence is suggested as an imaging biomarker with high specificity. Moreover, with multiple saturation powers, the exchange rate can be specifically obtained from AREX data and thus in principle pH changes in tissues can be detected without the influence of many other confounding effects.

Both the Bradford and BCA methods detect the total protein concentration in tissues, and because of the steps taken for protein extraction we cannot exclude the possible loss of water or some other sources of error. However, clearly there was no major variation between tumor and normal brain to explain the apparent large differences in CEST data with minor differences in protein concentration. A possible explanation is that APT contrast may arise from relatively mobile and accessible proteins and peptides only, not from total proteins. However, this needs be verified by more sophisticated biochemical experiments specifically targeting mobile proteins/peptides. In addition, another drawback of the biochemical methods used in the current work was that they measured total protein contents from tissue chunks collected from different regions in rat brains, by which the spatial information is lost. Proteomics analyses of the large-scale characteristics of the entire protein components of tissue can provide information about protein abundance and type (46), and 3D Matrix-assisted Laser Desorption/Ionization Imaging Mass Spectrometry (MALDI IMS) can be used to map specific proteins. Moreover, we have recently shown how to integrate 3D MALDI IMS of whole animal brain with high-resolution MRI (47). Therefore, additional studies correlating APT measurements and proteomic data may further elucidate the contrast mechanism underlying APT parameters.

While the current study promisingly examined the NOE centered at −3.5 ppm, the NOE centered at −1.6 ppm clearly differentiates tumors from contralateral normal brain tissues too. However, the underlying biophysical mechanism for this difference is not clear. Our previous studies suggest that it may originate with an immobilized metabolite, such as choline-containing compounds, that have strong magnetic coupling with water. In addition, there may be multiple sources of resonances near −1.6 ppm which can be revealed using different irradiation powers (48). Thus the NOE centered around −1.6 ppm might provide a new molecular imaging contrast for detecting or characterizing cancer. The NOE centered at −1.6 ppm is currently under further investigation.

Conclusions

High frequency resolution Z-spectra of rat gliomas were acquired *in vivo* at 9.4T. Different methods for quantifying APT and NOE contrasts were compared and correlated to several

conventional MR parameters, i.e. R_1, R_2, PSR, k_{mf} and ADC. After corrections for spillover, MT and R_1 relaxation effects, APT in tumors was found not significantly different from normal tissues but NOE effects at −3.5 ppm in tumors showed significant decreases compared with normal tissues. Biochemical measurements verify that there is no significant enhancement of protein contents in tumors, consistent with corrected APT measurements and previous literature. Our results may assist better understanding the contrast depicted by CEST imaging in tumors, and assist the development of improved APT and NOE measurements in cancer imaging.

Acknowledgments

This study was supported by NIH K25CA168936, R01CA109106, R01CA173593, R01EB000214 and P50CA128323. The authors thank Ms. Zou Yue for assistance in animal surgeries.

Abbreviations

CEST	chemical exchange saturation transfer
APT	amide proton transfer
NOE	nuclear Overhauser enhancement
AREX	apparent exchange-dependent relaxation
PSR	pool size ratio of macromolecular pool to free water pool in qMT
k_{mf}	MT exchange rate from macromolecular pool to free water pool

REFERENCES

1. Wolff SD, Balaban RS. NMR Imaging of Labile Proton-Exchange. J Magn Reson. 1990; 86(1):164–169.
2. Ward KM, Aletras AH, Balaban RS. A new class of contrast agents for MRI based on proton chemical exchange dependent saturation transfer (CEST). J Magn Reson. 2000; 143(1):79–87. [PubMed: 10698648]
3. Zhou JY, van Zijl PCM. Chemical exchange saturation transfer imaging and spectroscopy. Prog Nucl Magn Reson Spectrosc. 2006; 48(2–3):109–136.
4. van Zijl PC, Yadav NN. Chemical exchange saturation transfer (CEST): what is in a name and what isn't? Magn Reson Med. 2011; 65(4):927–948. [PubMed: 21337419]
5. Zhou J, Lal B, Wilson DA, Laterra J, van Zijl PC. Amide proton transfer (APT) contrast for imaging of brain tumors. Magn Reson Med. 2003; 50(6):1120–1126. [PubMed: 14648559]
6. Jones CK, Schlosser MJ, van Zijl PCM, Pomper MG, Golay X, Zhou JY. Amide proton transfer imaging of human brain tumors at 3T. Magn Reson Med. 2006; 56(3):585–592. [PubMed: 16892186]
7. Salhotra A, Lal B, Laterra J, Sun PZ, van Zijl PCM, Zhou JY. Amide proton transfer imaging of 9L gliosarcoma and human glioblastoma xenografts. NMR Biomed. 2008; 21(5):489–497. [PubMed: 17924591]
8. Jia GA, Abaza R, Williams JD, Zynger DL, Zhou JY, Shah ZK, Patel M, Sammet S, Wei L, Bahnson RR, Knopp MV. Amide Proton Transfer MR Imaging of Prostate Cancer: A Preliminary Study. J Magn Reson Imaging. 2011; 33(3):647–654. [PubMed: 21563248]
9. Zu ZL, Janve VA, Li K, Does MD, Gore JC, Gochberg DF. Multi-angle ratiometric approach to measure chemical exchange in amide proton transfer imaging. Magn Reson Med. 2012; 68(3):711–719. [PubMed: 22161770]
10. Jin T, Wang P, Zong X, Kim SG. MR imaging of the amide-proton transfer effect and the pH-insensitive nuclear overhauser effect at 9.4 T. Magn Reson Med. 2013; 69(3):760–770. [PubMed: 22577042]

11. Zu Z, Janve VA, Xu J, Does MD, Gore JC, Gochberg DF. A new method for detecting exchanging amide protons using chemical exchange rotation transfer. Magn Reson Med. 2013; 69(3):637–647. [PubMed: 22505325]
12. Scheidegger R, Vinogradov E, Alsop DC. Amide Proton Transfer Imaging With Improved Robustness to Magnetic Field Inhomogeneity and Magnetization Transfer Asymmetry Using Saturation With Frequency Alternating RF Irradiation. Magn Reson Med. 2011; 66(5):1275–1285. [PubMed: 21608029]
13. Zaiss M, Bachert P. Exchange-dependent relaxation in the rotating frame for slow and intermediate exchange - modeling off-resonant spin-lock and chemical exchange saturation transfer. NMR Biomed. 2013; 26(5):507–518. [PubMed: 23281186]
14. Jin, T.; Kim, SG. In vivo saturation transfer imaging of nuclear Overhauser effect from aromatic and aliphatic protons: implication to APT quantification. Salt Lake City: 2013 Apr. p. 2528
15. Cramer W. On the biochemical mechanism of growth. J Physiol. 1916; 50(5):322–334. [PubMed: 16993346]
16. Tozer DJ, Rees JH, Benton CE, Waldman AD, Jager HR, Tofts PS. Quantitative magnetisation transfer imaging in glioma: preliminary results. NMR Biomed. 2011; 24(5):492–498. [PubMed: 20960580]
17. Underhill HR, Rostomily RC, Mikheev AM, Yuan C, Yarnykh VL. Fast bound pool fraction imaging of the in vivo rat brain: association with myelin content and validation in the C6 glioma model. Neuroimage. 2011; 54(3):2052–2065. [PubMed: 21029782]
18. Xu J, Li K, Zu Z, Li X, Gochberg DF, Gore JC. Quantitative magnetization transfer imaging of rodent glioma using selective inversion recovery. NMR Biomed. (in press).
19. Saryan LA, Hollis DP, Economou JS, Eggleston JC. Nuclear magnetic resonance studies of cancer. IV. Correlation of water content with tissue relaxation times. J Natl Cancer Inst. 1974; 52(2):599–602. [PubMed: 4406036]
20. Damadian R. Tumor detection by nuclear magnetic resonance. Science. 1971; 171(3976):1151–1153. [PubMed: 5544870]
21. Jones CK, Huang A, Xu J, Edden RA, Schar M, Hua J, Oskolkov N, Zaca D, Zhou J, McMahon MT, Pillai JJ, van Zijl PC. Nuclear Overhauser enhancement (NOE) imaging in the human brain at 7T. Neuroimage. 2013; 77:114–124. [PubMed: 23567889]
22. van Zijl PCM, Zhou J, Mori N, Payen JF, Wilson D, Mori S. Mechanism of magnetization transfer during on-resonance water saturation. A new approach to detect mobile proteins, peptides, and lipids. Magn Reson Med. 2003; 49(3):440–449. [PubMed: 12594746]
23. Mori S, Berg JM, van Zijl PC. Separation of intramolecular NOE and exchange peaks in water exchange spectroscopy using spin-echo filters. Journal of Biomolecular NMR. 1996; 7(1):77–82. [PubMed: 8720834]
24. Gore JC, Brown MS, Armitage IM. An analysis of magnetic cross-relaxation between water and methylene protons in a model system. Magn Reson Med. 1989; 9(3):333–342. [PubMed: 2540400]
25. Ling W, Regatte RR, Navon G, Jerschow A. Assessment of glycosaminoglycan concentration in vivo by chemical exchange-dependent saturation transfer (gagCEST). Proc Natl Acad Sci U S A. 2008; 105(7):2266–2270. [PubMed: 18268341]
26. Liu D, Zhou J, Xue R, Zou Z, An J, Wang DJ. Quantitative characterization of nuclear Overhauser enhancement and amide proton transfer effects in the human brain at 7 tesla. Magn Reson Med. 2013 (In press).
27. Mougin O, Clemence M, Peters A, Pitiot A, Gowland P. High-resolution imaging of magnetisation transfer and nuclear Overhauser effect in the human visual cortex at 7 T. NMR Biomed. 2013 (In press).
28. Zaiss M, Kunz P, Goerke S, Radbruch A, Bachert P. MR imaging of protein folding in vitro employing Nuclear-Overhauser-mediated saturation transfer. NMR Biomed. 2013
29. Bradford MM. A rapid and sensitive method for the quantitation of microgram quantities of protein utilizing the principle of protein-dye binding. Analytical Biochemistry. 1976; 72(1–2):248–254. [PubMed: 942051]

30. Smith PK, Krohn RI, Hermanson GT, Mallia AK, Gartner FH, Provenzano MD, Fujimoto EK, Goeke NM, Olson BJ, Klenk DC. Measurement of protein using bicinchoninic acid. Analytical Biochemistry. 1985; 150(1):76–85. [PubMed: 3843705]
31. Colvin DC, Yankeelov TE, Does MD, Yue Z, Quarles C, Gore JC. New insights into tumor microstructure using temporal diffusion spectroscopy. Cancer Res. 2008; 68(14):5941–5947. [PubMed: 18632649]
32. Hu X, Le TH. Artifact reduction in EPI with phase-encoded reference scan. Magn Reson Med. 1996; 36(1):166–171. [PubMed: 8795036]
33. Kim M, Gillen J, Landman BA, Zhou J, van Zijl PC. Water saturation shift referencing (WASSR) for chemical exchange saturation transfer (CEST) experiments. Magn Reson Med. 2009; 61(6): 1441–1450. [PubMed: 19358232]
34. Gochberg DF, Gore JC. Quantitative imaging of magnetization transfer using an inversion recovery sequence. Magn Reson Med. 2003; 49(3):501–505. [PubMed: 12594753]
35. Li K, Zu Z, Xu J, Janve VA, Gore JC, Does MD, Gochberg DF. Optimized inversion recovery sequences for quantitative T1 and magnetization transfer imaging. Magn Reson Med. 2010; 64(2): 491–500. [PubMed: 20665793]
36. Ericsson C, Nister M. Protein extraction from solid tissue. Methods Mol Biol. 2011; 675:307–312. [PubMed: 20949398]
37. Maes F, Collignon A, Vandermeulen D, Marchal G, Suetens P. Multimodality image registration by maximization of mutual information. IEEE Trans Med Imaging. 1997; 16(2):187–198. [PubMed: 9101328]
38. Dula AN, Asche EM, Landman BA, Welch EB, Pawate S, Sriram S, Gore JC, Smith SA. Development of chemical exchange saturation transfer at 7 T. Magn Reson Med. 2011; 66(3):831–838. [PubMed: 21432902]
39. Rajan SS, Rosa L, Francisco J, Muraki A, Carvlin M, Tuturea E. MRI characterization of 9L-glioma in rat brain at 4.7 Tesla. Magn Reson Imaging. 1990; 8(2):185–190. [PubMed: 2338899]
40. Zhong JH, Gore JC, Armitage IM. Relative contributions of chemical exchange and other relaxation mechanisms in protein solutions and tissues. Magn Reson Med. 1989; 11(3):295–308. [PubMed: 2550719]
41. Zhou J, Hong X, Zhao X, Gao JH, Yuan J. APT-weighted and NOE-weighted image contrasts in glioma with different RF saturation powers based on magnetization transfer ratio asymmetry analyses. Magn Reson Med. 2013; 70(2):320–327. [PubMed: 23661598]
42. Neuhaus, D.; Williamson, MP. The nuclear Overhauser effect in structural and conformational analysis. Vol. xxvii. New York: Wiley; 2000. p. 619
43. Wüthrich, K. NMR of proteins and nucleic acids. Vol. xv. New York: Wiley; 1986. p. 292
44. Desmond KL, Moosvi F, Stanisz GJ. Mapping of amide, amine, and aliphatic peaks in the CEST spectra of murine xenografts at 7 T. Magn Reson Med. 2013
45. Wu R, Liu CM, Liu PK, Sun PZ. Improved measurement of labile proton concentration-weighted chemical exchange rate (k(ws)) with experimental factor-compensated and T(1) -normalized quantitative chemical exchange saturation transfer (CEST) MRI. Contrast Media Mol Imaging. 2012; 7(4):384–389. [PubMed: 22649044]
46. Seeley EH, Caprioli RM. Molecular imaging of proteins in tissues by mass spectrometry. Proc Natl Acad Sci U S A. 2008; 105(47):18126–18131. [PubMed: 18776051]
47. Sinha TK, Khatib-Shahidi S, Yankeelov TE, Mapara K, Ehtesham M, Cornett DS, Dawant BM, Caprioli RM, Gore JC. Integrating spatially resolved three-dimensional MALDI IMS with in vivo magnetic resonance imaging. Nature Methods. 2008; 5(1):57–59. [PubMed: 18084298]
48. Zu, Z.; Xu, J.; Li, H.; Quarles, CC.; Does, MD.; Gore, JC.; Gochberg, DF. Imaging of Amide Proton Transfer (APT) and Nuclear Overhauser Effect (NOE) Using Chemical Exchange Rotation Transfer (CERT). Salt Lake City: 2013 Apr. p. 4241

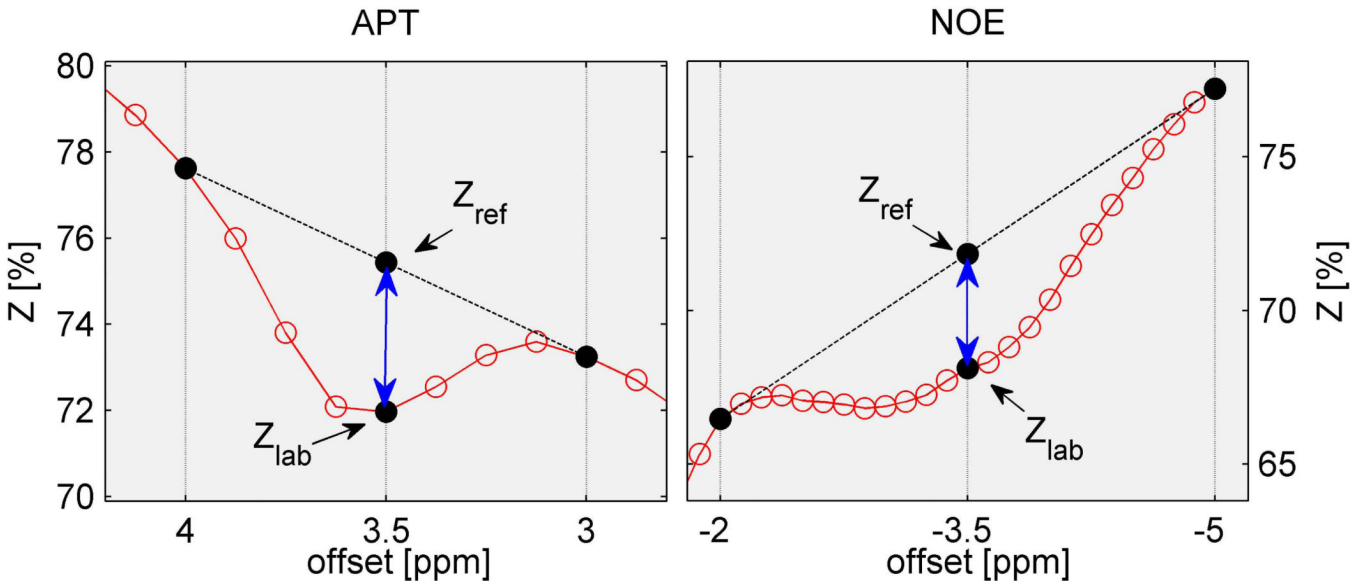

Figure 1.
Illustration of the three-offset method used for APT and NOE quantification. The Z-spectrum (circles) was measured from a rat 9L glioma tumor in vivo. Z_{ref}(3.5 ppm)=[Z (4.0 ppm) + Z (3.0 ppm)] / 2, and Z_{ref}(−3.5 ppm)=[Z (−2.0 ppm) + Z (−5.0 ppm)] / 2.

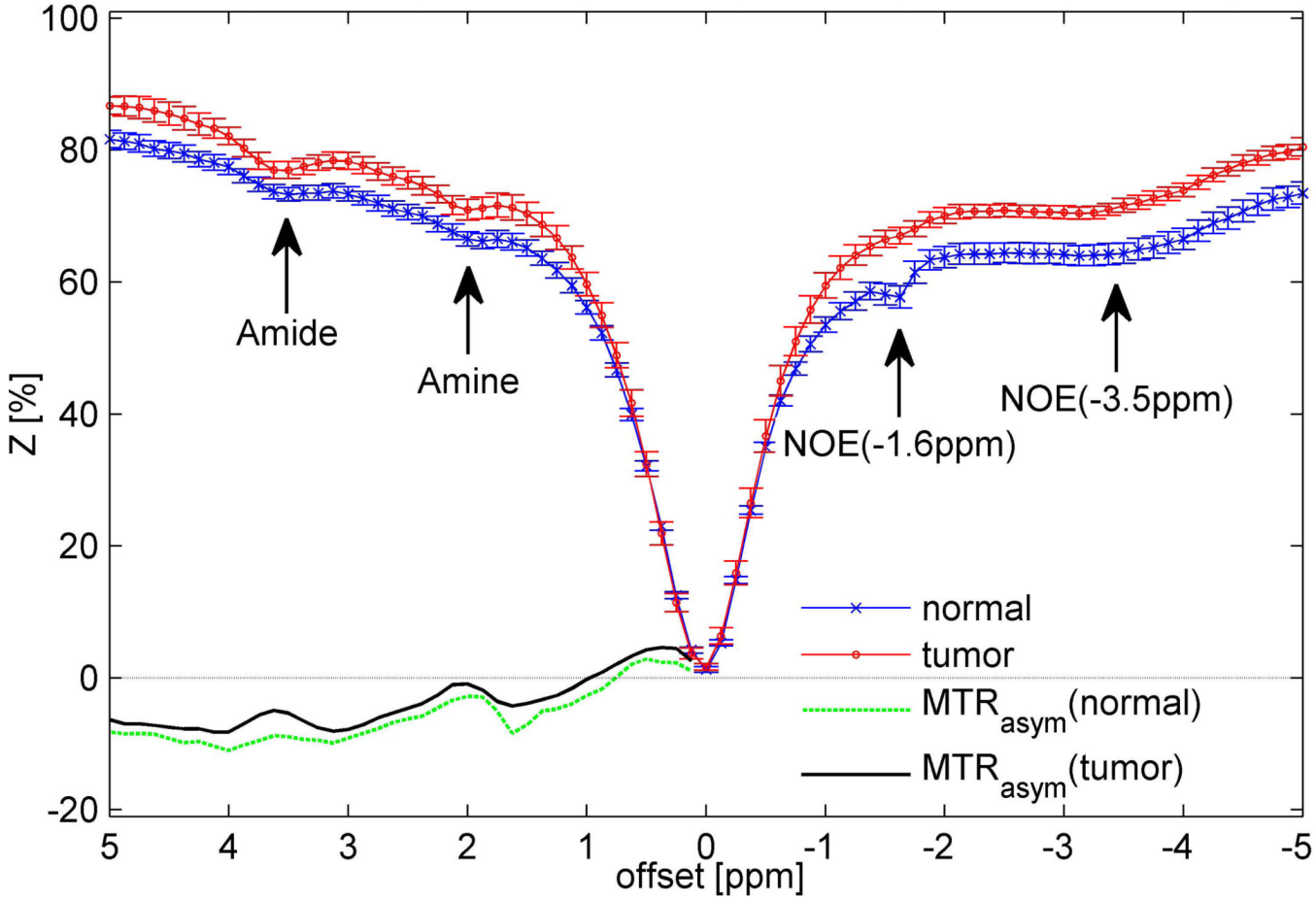

Figure 2.

Representative Z-spectra of a 9L glioma tumor and contralateral normal brain tissue from a rat. MTR_{asym}, the subtraction of downfield spectra from upfield, shows the conventional APT contrast obtained using the asymmetry analysis. The error bars represent standard deviations of ROIs.

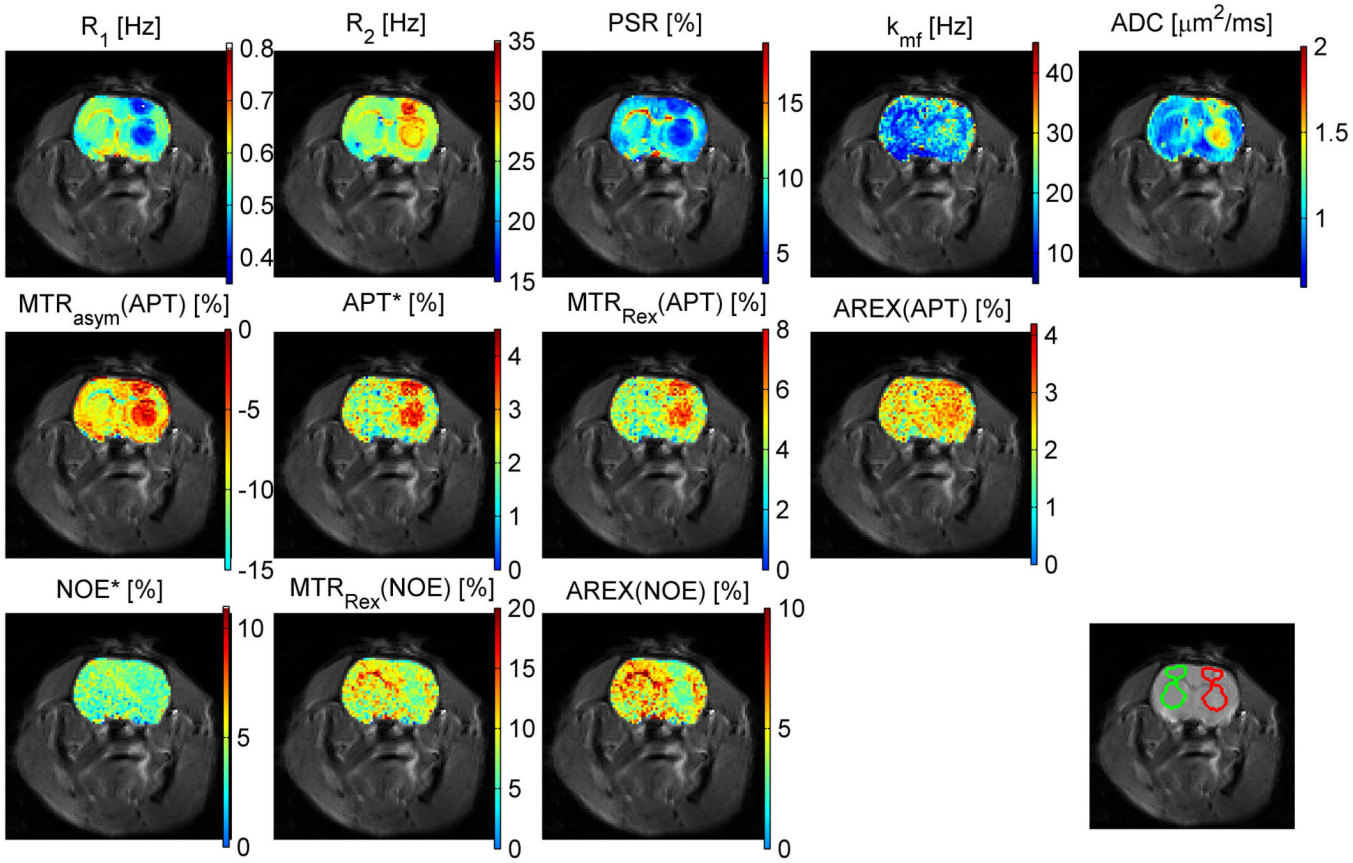

Figure 3.

Multiple MR parametric maps of a representative rat overlaid on a corresponding 2-shot spin-echo EPI image. The lower right image shows the ROIs of tumor (red) and contralateral normal tissue (green). Note that the 9L glioma tumor is in the right hemisphere, and mirrored ROI in the left hemisphere is the contralateral normal tissue region.

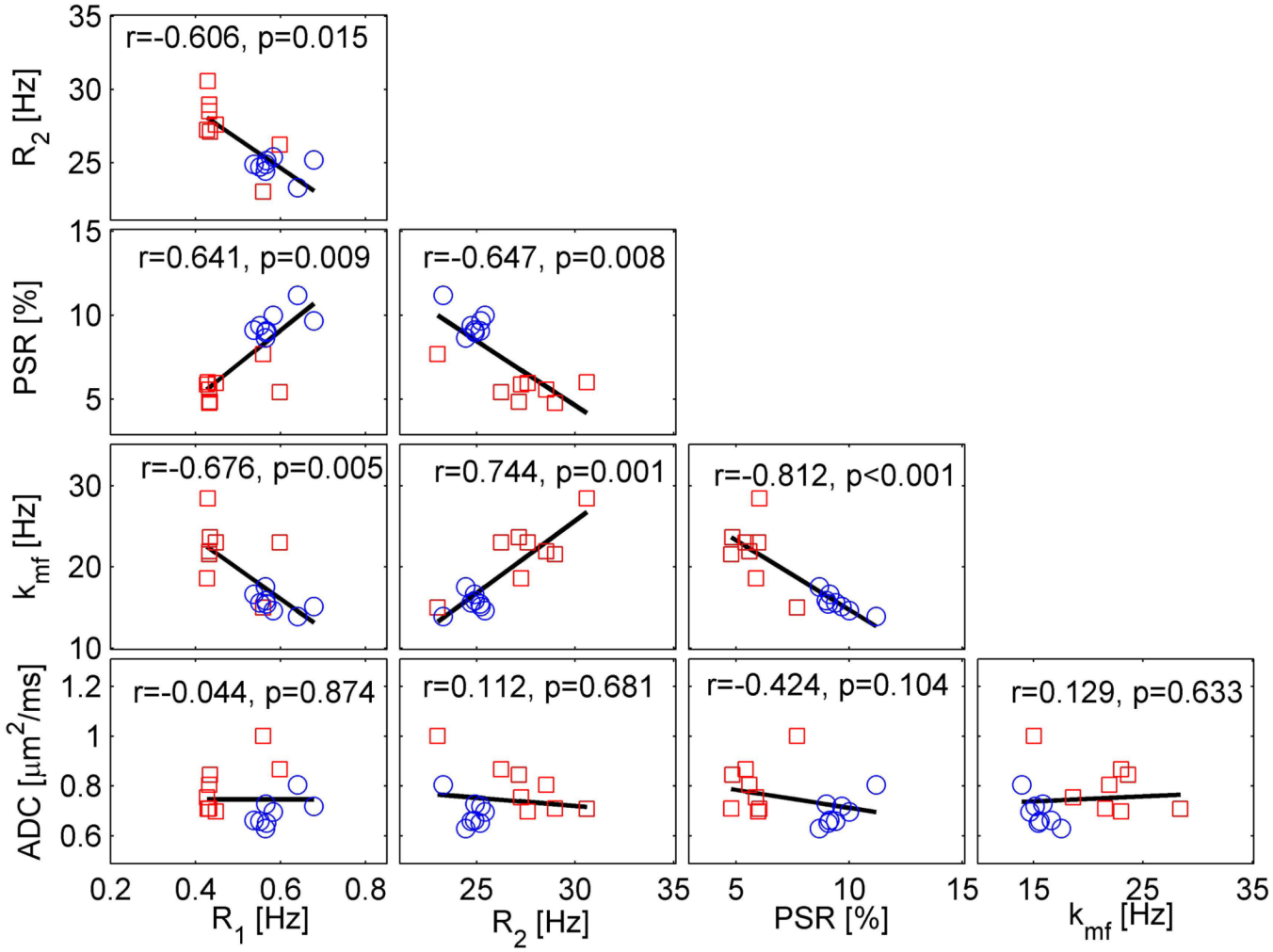

Figure 4.

Summary of correlations of five conventional MRI parameters (R_1, R_2, PSR, k_{mf} and ADC), respectively, of all eight rats. The red squares represent the mean values of each tumor, and blue circles are mean values of each ROI of contralateral normal tissue. The Spearman's rank correlation coefficient (r) and p-value of each correlation are provided. The solid lines represent the linear regression of all data points in each correlation sub-figure.

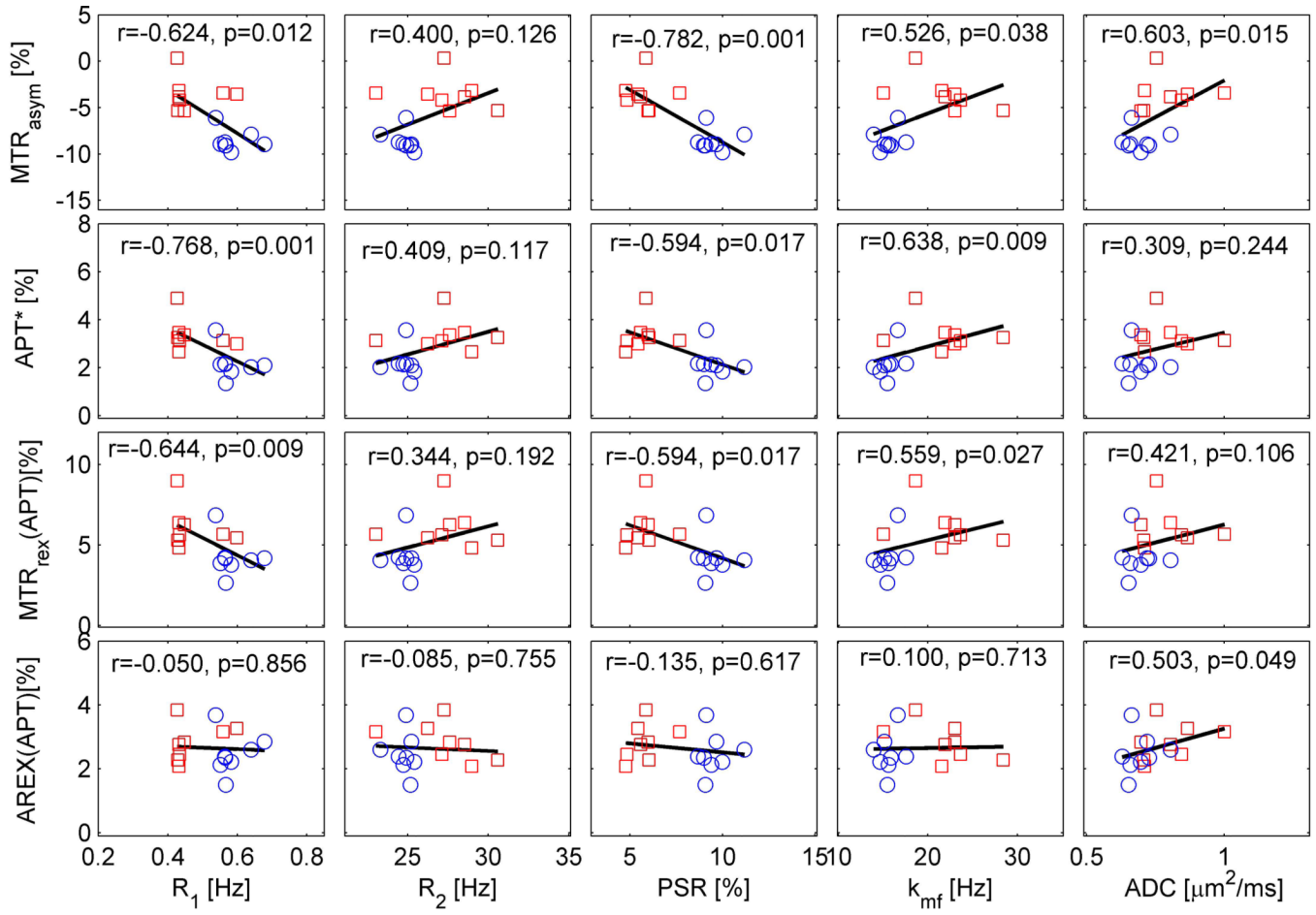

Figure 5.

Summarized correlation of four CEST parameters (MTR_{asym}, APT*, MTR_{Rex}(APT) and AREX(APT)) with five conventional MRI parameters (R_1, R_2, PSR, k_{mf} and ADC), respectively, of all eight rats. The legends are the same as in Figure 4.

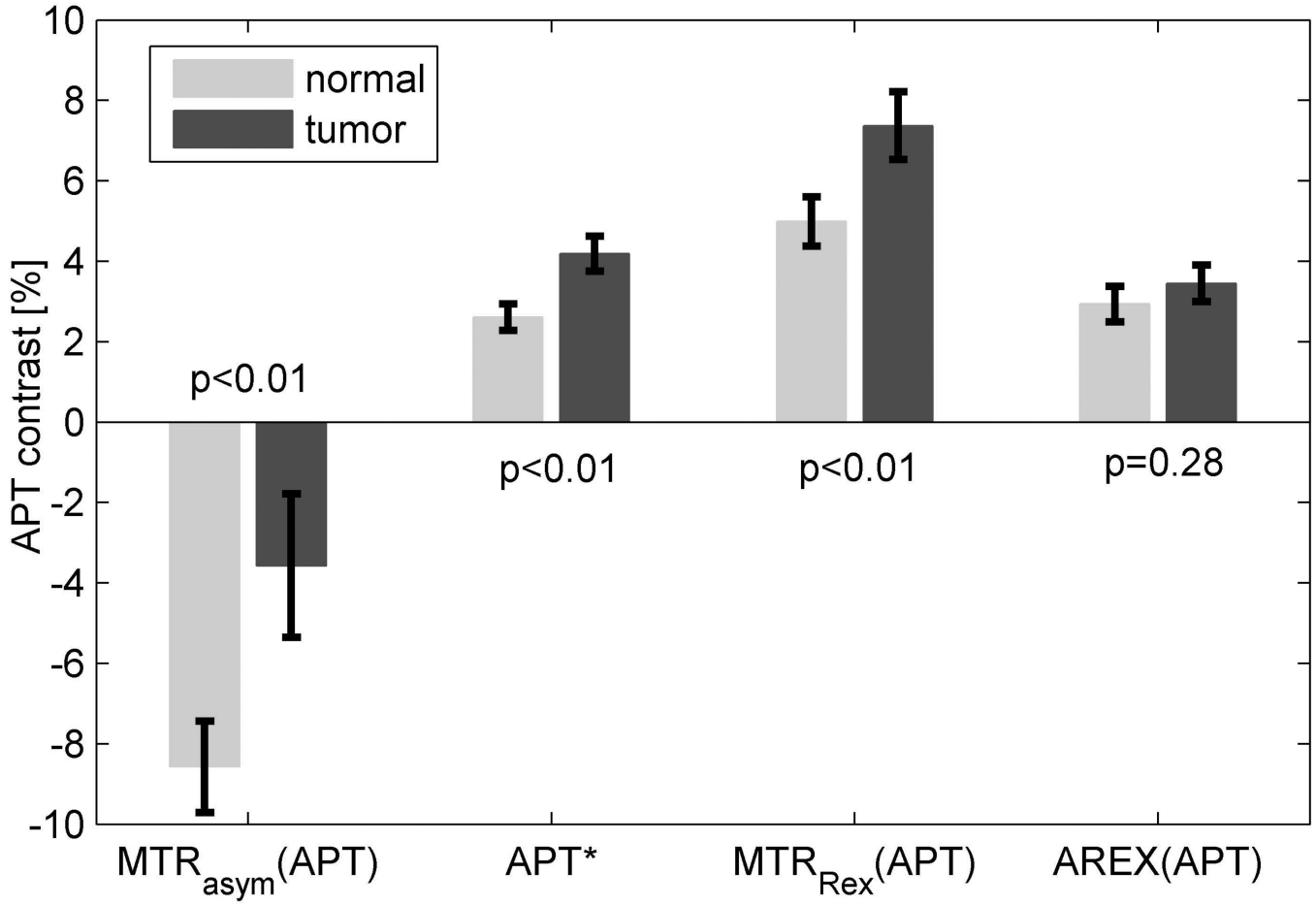

Figure 6.
Summary of four APT parameters (MTR_{asym}, APT*, MTR_{Rex}(APT) and AREX(APT)) of all eight rats to differentiate tumors from normal tissues. The p value of the Wilcoxon rank-sum test is shown for each comparison pair.

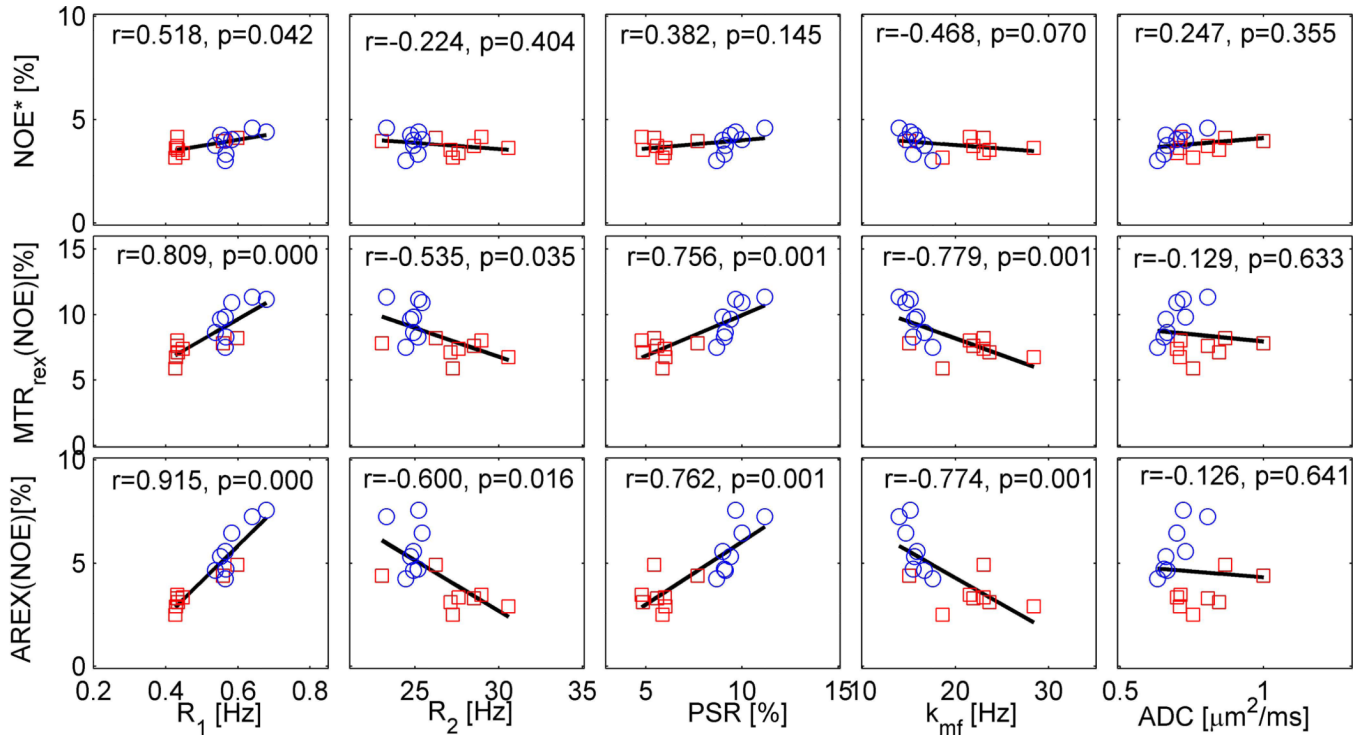

Figure 7.

Summary of correlations between three NOE parameters (NOE*, MTR_{Rex}(NOE) and AREX(NOE)) and five conventional MRI parameters (R_1, R_2, PSR, k_{mf} and ADC), respectively, of all eight rats. The legends are the same as in Figure 4.

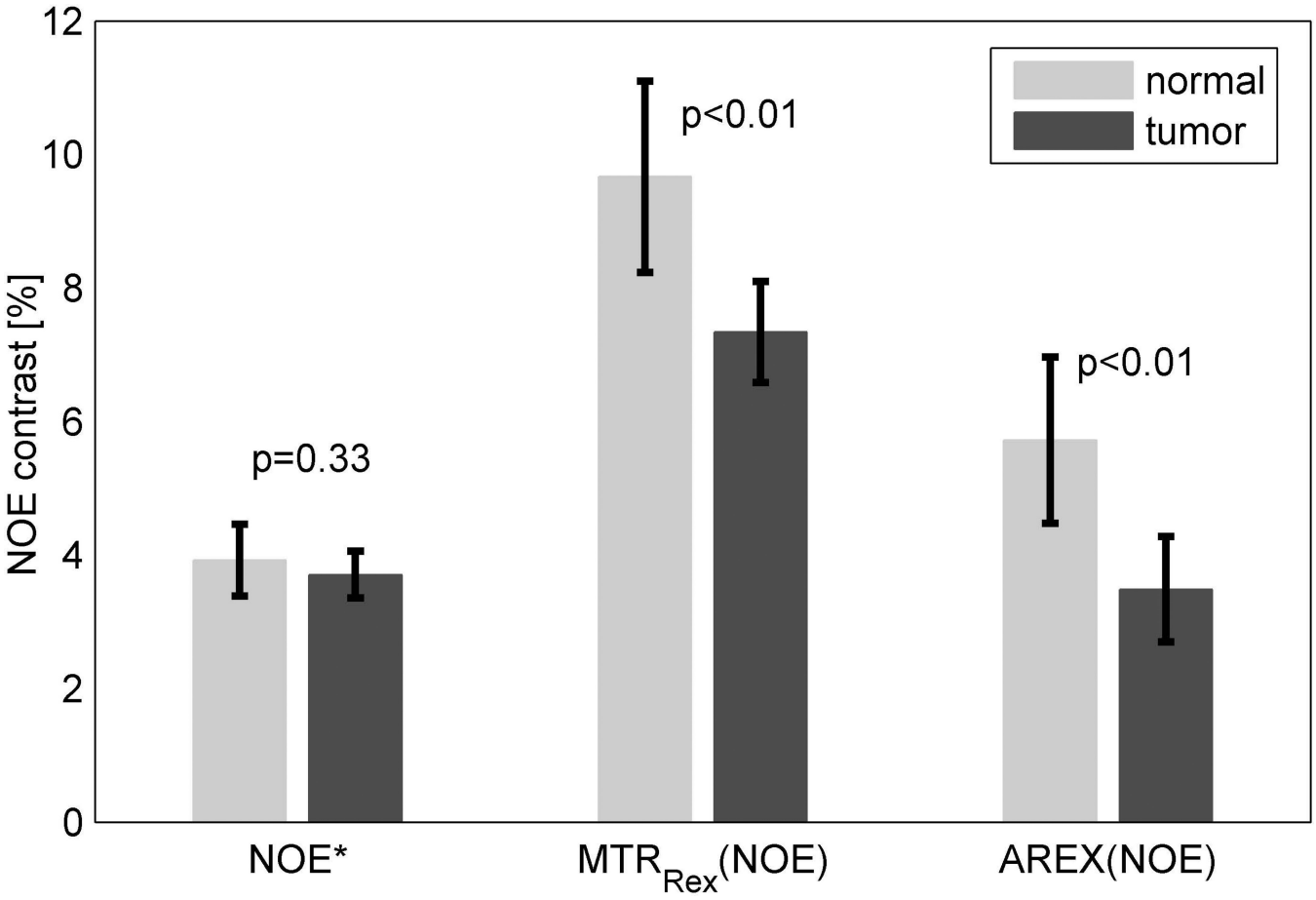

Figure 8.
Summary of three NOE parameters (NOE*, MTR_{Rex}(NOE) and AREX(NOE)) of all eight rats to differentiate tumor from normal tissue. The p value of the Wilcoxon rank-sum test is provided for each comparison pair.

Table 1

Summarized results of protein measurements using biochemical measurements and APT measurements.

	Protein contents		APT measurements			
	Bradford [‰]*	**BCA [‰]***	**MTR_{asym} [%]**	**APT* [%]**	**MTR_{Rex}(APT) [%]**	**AREX(APT) [%]**
normal	95.60±7.13	106.50±11.80	−8.57±1.13	2.17±0.62	4.22±1.18	2.46±0.63
tumor	104.04±9.22	109.30±12.60	−3.57±1.78	3.36±0.66	6.06±1.28	2.83±0.58
p**	0.093	0.394	0.0002	0.007	0.007	0.279

* total weight of protein (μg) / total weight of tissue (mg)

** p is given by the Wilcoxon rank-sum test of tumor vs contralateral normal tissue in each column.